Article

Theoretical Research on Flow and Heat Transfer Characteristics of Hydrostatic Oil Film in Flat Microfluidic Boundary Layer

Liansheng Liu [1,2], Huiru Qu [1], Runze Duan [1,2,*], Teng Liu [3,*], Chentao Li [3], Enyu Wang [1] and Lujia Liu [4]

[1] School of Energy and Environmental Engineering, Hebei University of Technology, Tianjin 300401, China; liuliansheng@hebut.edu.cn (L.L.); quhuiru56@163.com (H.Q.); wey@hebut.edu.cn (E.W.)
[2] Hebei Key Laboratory of Thermal Science and Energy Clean Utilization, Tianjin 300401, China
[3] School of Mechanical Engineering, Hebei University of Technology, Tianjin 300401, China; lichentao2022@163.com
[4] Institute of Fundamental Technological Research, Polish Academy of Sciences, Pawińskiego 5b, 02-106 Warsaw, Poland; lujialiu@ippt.pan.pl
[*] Correspondence: duanrunze@hebut.edu.cn (R.D.); wuqiu-liu@163.com (T.L.)

Abstract: The hydrostatic bearing is the core component of ultra-precision computer numerical control (CNC) machine tools. Because the temperature rise in the oil film of hydrostatic bearings seriously affects the working accuracy of the bearings, it is important to study the flow and heat transfer characteristics of the oil film. Based on the physical model of an incompressible viscous fluid flowing in a flat microfluidic boundary layer, velocity, temperature and heat flux distribution equations of oil film are constructed by theories of heat transfer and hydrodynamics. Then, the effects of several parameters on velocity distribution, temperature distribution and heat flux distribution are analyzed, such as the upper plate velocity, the channel length, and so on. The results show that the dimensionless velocity of the oil film decreases with the increase in the upper plate velocity and the channel length. The oil film temperature distribution can be divided into three zones: the increasing zone, stabilizing zone and decreasing zone. The heat flux decreases linearly with the increase in the plate thickness, and increases linearly with the increase in the temperature difference.

Keywords: microfluidic boundary layer; hydrostatic oil film; velocity; temperature; heat flux

1. Introduction

Hydrostatic bearings, with the characteristics of high load-carrying properties, steady operation and low friction resistance, are widely used in heavy-duty high-precision equipment, and have become the core component of ultra-precision computer numerical control (CNC) machine tools [1–4]. The hydrostatic bearing in a hydrostatic turntable is shown in Figure 1. The hydrostatic bearing sends the hydraulic oil with a certain pressure to the oil chamber of the bearing to form a pressure oil film by using an oil supply device. Then, the pressure difference between the oil chambers forms the bearing capacity for floating the main shaft and supporting the external load, as shown in Figure 1b [3]. However, during the operation of the hydrostatic turntable, the velocity difference between the moving upper guide rail and the stationary axial bearing (or the moving lower guide rail and the stationary radial bearing) will be transmitted to the oil film. The viscous shear force, due to the existence of the velocity difference, converts mechanical energy into heat energy through frictional power consumption. On the one hand, the temperature of the hydraulic oil is increased, and the viscosity is correspondingly reduced, which leads to the change in the flow field state and the decline of the bearing performance [5]. On the other hand, the thermal deformation of the parts is forced to occur, in which the shape and gap of the oil film are forced to change [6]. These two aspects can affect the working accuracy of bearings.
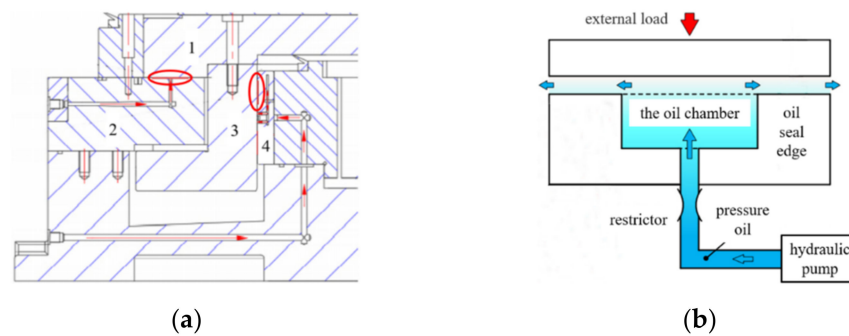
(a)   (b)

Figure 1. Hydrostatic bearing in hydrostatic turntable. 1. upper guide rail, 2. axial bearing, 3. lower guide rail, 4. radial bearing. (**a**) Internal oil circuit of hydrostatic turntable. (**b**) Schematic diagram of oil film.

In recent years, the oil film of bearings has been studied by many scholars from many aspects, such as thickness, bearing capacity and pressure distribution. The effects of working load, rotational speed, restrictor design parameters, lubricating oil viscosity and cutting force on oil film thickness have all been studied [7–10]. The results showed that the oil film thickness decreased with the increase in the working load, rotational speed or viscosity. The correct selection of the restrictor design parameters was essential to maintain oil film thickness. The effects of the oil supply pressure and oil film clearance on the dynamic characteristics and radial runout of the spindle were studied [11]. The research results suggested that the oil film clearance had a greater influence on the spindle runout. The minimum oil film of hydrostatic thrust bearings was determined by numerical methods and were approximately equal to the surface roughness [12]. In order to measure the oil film thickness, a promising non-invasive method and a practical schedule for the on-line reconstruction of the incident signal were proposed [13,14]. The effects of the wall slip, width-to-diameter ratio, eccentricity and other parameters on the bearing capacity of oil film were analyzed [15–17]. The research results indicated that wall slip, width-to-diameter ratio, eccentricity and oil inlet position angle can have a greater influence on the bearing capacity of oil film, while the oil inlet pressure was negligible. The effects of different oil cavity structures of four kinds of hydrodynamic-hydrostatic bearings with orifice throttling on oil film characteristics were analyzed [18]. The results showed that the reasonable oil cavity shape and restrictor design parameters can improve the bearing capacity. The bearing capacity of the oil film was improved by optimizing the oil film characteristic parameters of the hydrodynamic-hydrostatic bearings with capillary throttle [19]. When the hydrostatic guide model was established, the static bearing effect, extrusion effect, compression effect and inertia effect of the oil film were considered [20]. It was found that the best way to study the dynamic performance of the hydrostatic support was to simplify the spring damping system with mass. The effects of the rotational speed and lubricating oil viscosity on oil film pressure were studied [21,22]. The results showed that the viscosity had a great influence on the oil film pressure distribution of the heavy hydrostatic bearings, especially at high velocity, and the velocity of 8 rpm was key in the effect of rotational speed on oil film pressure. The effect of the inlet flow on the temperature field of the heavy hydrostatic bearings was studied [23]. The effects of the radial load on oil film pressure and temperature were studied [24]. The results reflected that the oil film pressure and temperature increased with the increase in the radial load at a constant velocity. The pressure field and velocity field of the oil film were studied and the behavior of the lubricating oil inside the oil film was qualitatively analyzed [25]. In order to obtain the oil film transient flow field, new dynamic mesh algorithms were proposed and can obtain the optimal mesh quality at any time step [26,27]. The fluid flow states in hydrostatic bearing at different fluid flows were studied [28]. The results showed that the transition in critical inlet fluid flow from laminar to turbulent was 22 L/min when the rotational speed of the table was 6 rpm. Heavy load characteristics of the oil film of hydrostatic thrust

bearings with a double rectangular cavity were studied [29]. It was found that the oil was extruded and seriously heated, and the viscosity dropped sharply under a heavy load.

　　In the theoretical works cited above, extensive research on oil film thickness and oil film bearing capacity was carried from multiple angles, but studies of the flow and heat transfer characteristics of oil film are less numerous. However, the flow and heat transfer characteristics of oil film affect the working accuracy of the hydrostatic bearing. Therefore, it is necessary to systematically study the flow and heat transfer characteristics of hydrostatic oil film. In this article, the hydrostatic oil film formed at the contact surface of the upper guide rail and the axial bearing (or the lower guide rail and the radial bearing) is considered. Then, the flow and heat transfer theories on the hydrostatic oil film are derived. Finally, the effects of some parameters on the velocity distribution, temperature distribution and heat flux distribution are investigated, such as the upper plate velocity, the channel length.

2. Physical Model

　　The length of the hydrostatic oil film formed between the upper guide rail and the axial bearing is 3–4 mm, and the thickness is 20 μm. VG10 hydraulic oil moves between the upper plate and the lower plate with a distance of 20 μm, enters from the left side of the plate and exits from the right side as shown in Figure 2. There is a pressure difference along the x-axis, with the pressure on the left and right being p_1 and p_2, respectively ($p_1 > p_2$). There is also a velocity difference along the y-axis, and the velocity of the upper plate and the lower plate are U and 0, respectively, as shown in Figure 3a. The temperatures of hydraulic oil and air (environment) are different, so there is heat transfer between hydraulic oil and air through the lower plate, as shown in Figure 3b. The upper plate is the same as the lower plate, as shown in Figure 3c. Parameter values of hydrostatic bearing are shown in Table 1.

Table 1. Parameter values in the hydrostatic bearing.

| Design Parameters		Values
The lower plate (stationary)	Thickness δ_1	0.3–0.5 m
	Inside temperature T_{W1}	19–21 °C
The upper plate (motion)	Thickness δ_2	0.1–0.2 m
	Inside temperature T_{W2}	$T_{W1} = T_{W2}$
	Velocity U	0–5 m/min
The channel between the upper and lower plates	Thickness δ	0.02 mm
	Length l	3–4 mm
	Pressure on the left p_1	2 MPa
	Pressure on the right p_2	0
VG10 hydraulic oil	Dynamic viscosity μ	0.0258 Pa·s
	Heat transfer coefficient k	0.13 W/(m·k)
Plate	Material	QT500
	Thermal conductivity λ	42.44 W/(m·k)
	Heat transfer coefficient with air h	5 W/(m²·k)
Air (ambient) temperature T_f		18–20 °C
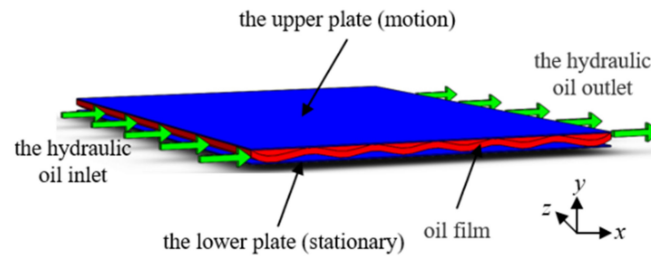
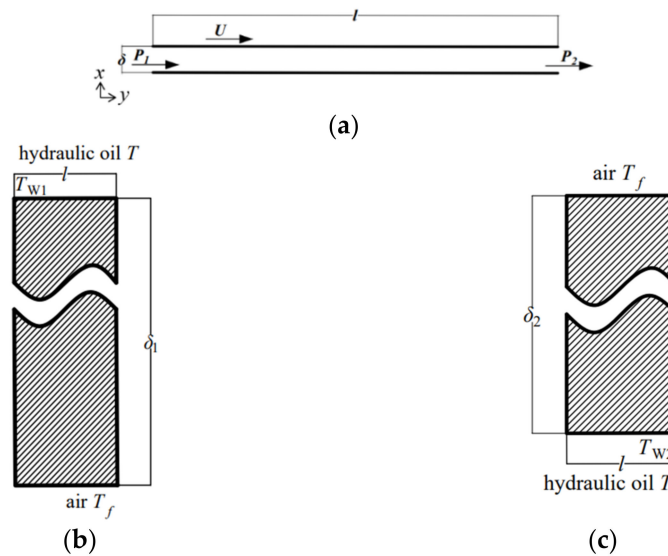**Figure 2.** The three-dimensional model of oil film.

Figure 3. Schematic diagram of two-dimensional physical model. (**a**) The two-dimensional model of oil film. (**b**) Lower plate. (**c**) Upper plate.

3. Mathematical Model

3.1. Velocity Distribution Model

Because the hydrostatic oil film thickness is 20 μm, which is much smaller than the boundary layer thickness, the hydraulic oil flows in the boundary layer and its viscosity must be considered. The hydraulic oil is an incompressible fluid, which means that ρ = const. The continuity equation and momentum equation of hydraulic oil are shown below:

$$\frac{\partial u}{\partial x} + \frac{\partial v}{\partial y} = 0 \tag{1}$$

$$\frac{\partial u}{\partial t} + u\frac{\partial u}{\partial x} + v\frac{\partial v}{\partial y} = f_x - \frac{1}{\rho}\frac{\partial p}{\partial x} + \nu\left(\frac{\partial^2 u}{\partial x^2} + \frac{\partial^2 u}{\partial y^2}\right) \tag{2}$$

$$\frac{\partial v}{\partial t} + u\frac{\partial v}{\partial x} + v\frac{\partial v}{\partial y} = f_y - \frac{1}{\rho}\frac{\partial p}{\partial y} + \nu\left(\frac{\partial^2 v}{\partial x^2} + \frac{\partial^2 v}{\partial y^2}\right) \tag{3}$$

where u is the velocity along the x-axis direction and v is the velocity along the y-axis direction. f_x is the force along the x-axis, and f_y is the force along the y-axis. ν is the kinematic viscosity of hydraulic oil. $\partial p / \partial x$ is the pressure gradient along the x-axis, and $\partial p / \partial y$ is the pressure gradient along the y-axis.

Because the velocity of the hydraulic oil is small, it is generally considered that the flow of hydraulic oil between the upper and lower plates is laminar flow [3], which means

that the velocity v along the y-axis can be ignored. Meanwhile, the hydraulic oil is a steady flow, and Equations (1)–(3) can be written as:

$$f_x - \frac{1}{\rho}\frac{\partial p}{\partial x} + \nu\frac{\partial^2 u}{\partial y^2} = 0 \tag{4}$$

$$f_y - \frac{1}{\rho}\frac{\partial p}{\partial y} = 0 \tag{5}$$

The gravity of the hydraulic oil is considered, which means that $f_x = 0$ and $f_y = -g$, then Equations (4) and (5) can be written as:

$$\frac{\partial^2 u}{\partial y^2} = \frac{1}{\mu}\frac{\partial p}{\partial x} \tag{6}$$

$$p = -\rho g y + f(x) \tag{7}$$

The oil film pressure gradient can be written as:

$$\frac{\partial p}{\partial x} \approx \frac{\Delta p}{\Delta x} = \frac{p_2 - p_1}{l} \tag{8}$$

The boundary conditions of velocity are:

$$y = 0,\ u = 0,\ y = \delta,\ u = U \tag{9}$$

Substituting Equations (8) and (9) into Equation (6), it can be obtained as:

$$u = \frac{U}{\delta}y + \frac{1}{2\mu}\frac{p_2 - p_1}{l}\left(y^2 - \delta y\right) \tag{10}$$

Equation (10) is dimensionless and can be written as:

$$\frac{u}{U} = \frac{y}{\delta} + \mathrm{P}\frac{y}{\delta}\left(1 - \frac{y}{\delta}\right) \tag{11}$$

where $P = -\frac{\delta^2}{2\mu U}\frac{p_2 - p_1}{l}$ is the dimensionless pressure.

Substituting the parameter values in Table 1 into Equation (11), the oil film velocity distribution equation can be obtained:

$$\frac{u}{U} = \frac{y}{\delta} + \frac{1.55 \times 10^{-2}}{Ul}\frac{y}{\delta}\left(1 - \frac{y}{\delta}\right) \tag{12}$$

3.2. Temperature Distribution Model

The continuity equation, momentum equation and energy equation of VG10 hydraulic oil flowing in the plate microflow boundary layer are obtained:

$$\frac{\partial u}{\partial x} + \frac{\partial v}{\partial y} = 0 \tag{13}$$

$$\frac{\partial u}{\partial t} + u\frac{\partial u}{\partial x} + v\frac{\partial v}{\partial y} = f_x - \frac{1}{\rho}\frac{\partial p}{\partial x} + \nu\left(\frac{\partial^2 u}{\partial x^2} + \frac{\partial^2 u}{\partial y^2}\right) \tag{14}$$

$$\frac{\partial v}{\partial t} + u\frac{\partial v}{\partial x} + v\frac{\partial v}{\partial y} = f_y - \frac{1}{\rho}\frac{\partial p}{\partial y} + \nu\left(\frac{\partial^2 v}{\partial x^2} + \frac{\partial^2 v}{\partial y^2}\right) \tag{15}$$

$$\rho\frac{De}{Dt} = div(k\nabla T) + \mathbf{P} \times \nabla\mathbf{u} \tag{16}$$

where e is the internal energy per unit volume, $\frac{De}{Dt} = \frac{\partial e}{\partial t} + u\frac{\partial e}{\partial x} + v\frac{\partial e}{\partial y}$, k is the heat transfer coefficient, stress component $\mathbf{P} = \begin{bmatrix} \sigma_{xx} & \tau_{xy} \\ \tau_{yx} & \sigma_{yy} \end{bmatrix}$, velocity $\mathbf{u} = (u, v)$.

In Equation (16):

$$\mathbf{P} \times \nabla\mathbf{u} = \frac{\partial\left(u\sigma_{xx} + v\tau_{xy}\right)}{\partial x} + \frac{\partial\left(u\tau_{yx} + v\sigma_{yy}\right)}{\partial y} \tag{17}$$

$$div(k\nabla T) = k\left(\frac{\partial^2 T}{\partial x^2} + \frac{\partial^2 T}{\partial y^2}\right) \tag{18}$$

According to Newton's law of internal friction, Equation (17) and internal energy can be written as:

$$\mathbf{P} \times \nabla\mathbf{u} = \frac{\partial(-pu)}{\partial x} + \mu\frac{\partial\left(2u\frac{\partial u}{\partial x}\right)}{\partial x} + \mu\frac{\partial\left(u\frac{\partial u}{\partial y}\right)}{\partial y} \tag{19}$$

$$\frac{De}{Dt} = \frac{\partial e}{\partial t} + u\frac{\partial e}{\partial x} \tag{20}$$

$\frac{\partial u}{\partial x} = \frac{\partial^2 u}{\partial x^2} = 0$ can be known from Equation (12), Equation (19) can be obtained as:

$$\mathbf{P} \times \nabla\mathbf{u} = -u\frac{\partial p}{\partial x} + \mu\left[u\frac{\partial^2 u}{\partial y^2} + \left(\frac{\partial u}{\partial y}\right)^2\right] \tag{21}$$

Substituting Equations (18), (20) and (21) into Equation (16), the energy equation can be written as:

$$\rho\left(\frac{\partial e}{\partial t} + u\frac{\partial e}{\partial x}\right) = k\left(\frac{\partial^2 T}{\partial x^2} + \frac{\partial^2 T}{\partial y^2}\right) - u\frac{\partial p}{\partial x} + \mu\left[u\frac{\partial^2 u}{\partial y^2} + \left(\frac{\partial u}{\partial y}\right)^2\right] \tag{22}$$

The oil film flow is steady and fully developed, then:

$$\frac{\partial e}{\partial t} = 0, \ \frac{\partial e}{\partial x} = 0, \ \frac{\partial^2 T}{\partial x^2} = 0 \tag{23}$$

Equation (22) can be written as:

$$0 = k\frac{\partial^2 T}{\partial y^2} - u\frac{\partial p}{\partial x} + \mu\left[u\frac{\partial^2 u}{\partial y^2} + \left(\frac{\partial u}{\partial y}\right)^2\right] \tag{24}$$

After calculating the first and second derivatives of velocity from Equation (12), Equation (24) can be obtained as:

$$T = -\frac{\mu^3}{12k}\left(\frac{\partial x}{\partial p}\right)^2\left[\frac{1}{\mu}\frac{\partial x}{\partial p}y - \left(\frac{1}{2\mu}\frac{\partial x}{\partial p}\delta - \frac{U}{\delta}\right)\right]^4 + C_1 y + C_2 \tag{25}$$

The boundary conditions of temperature are:

$$y = 0, \ T = T_{w1}, \ y = \delta, \ T = T_{w2} = T_{w1} \tag{26}$$

C_1 and C_2 can be solved as:

$$C_1 = \frac{U}{\delta}\frac{\mu^2}{3k}\left(\frac{\partial x}{\partial p}\right) \times \left[\left(\frac{1}{2\mu}\frac{\partial x}{\partial p}\delta\right)^2 + \left(\frac{U}{\delta}\right)^2\right] \tag{27}$$

$$C_2 = T_{w1} + \frac{\mu^3}{12k}\left(\frac{\partial x}{\partial p}\right)^2\left(\frac{1}{2\mu}\frac{\partial x}{\partial p}\delta - \frac{U}{\delta}\right)^4 \tag{28}$$

By substituting the parameter values in Table 1 into Equations (25), (27) and (28), the temperature distribution equation is obtained as follows:

$$T = -2.75 \times 10^{-18} l^2 \left(-\frac{7.75 \times 10^7}{l} y + \frac{776}{l} + 5 \times 10^4 U \right)^4 + C_1 y + C_2 \tag{29}$$

where

$$C_1 = -4.27 \times 10^{-5} U l \times \left[(776/l)^2 + \left(5 \times 10^4 U \right)^2 \right] \tag{30}$$

$$C_2 = T_{w1} + 2.75 \times 10^{-18} l^2 \times \left(776/l + 5 \times 10^4 U \right)^4 \tag{31}$$

3.3. Heat Flux Distribution Model

The heat transfer process between hydraulic oil and surrounding air through the plate can be divided into three links connected in series. The first link is the heat conduction process between hydraulic oil and the inside of the plate, and is not considered. The second link is the heat conduction process of the inside and outside of the plate. The third link is the heat convection process between the outside of the plate and the surrounding air.

The heat flux of the heat conduction process and the heat convection process of the lower plate can be written as:

$$q_1 = \lambda \frac{T_{w1} - T_{w3}}{\delta_1}, \; q_1 = h \left(T_{w3} - T_f \right) \tag{32}$$

Because the above two processes are steady-state processes with the same heat flux, the heat flux distribution equation of the lower plate can be obtained as follows:

$$q_1 = \frac{T_{w1} - T_f}{\frac{\delta_1}{42.22} + 0.2} \tag{33}$$

The derivation process of the heat flux distribution equation of the upper plate is the same as that of the lower plate. Therefore, the heat flux distribution equation of the upper plate can be directly written as:

$$q_2 = \frac{T_{w2} - T_f}{\frac{\delta_2}{42.22} + 0.2} \tag{34}$$

According to Equations (33) and (34), there are two parameters affecting the heat flux of the plate, which are the plate thickness (δ_1, δ_2) and the temperature difference between the inside temperature of the plate and the environment temperature ($\Delta T_1 = T_{W1} - T_f$, $\Delta T_2 = T_{W2} - T_f$).

4. Results and Discussion

4.1. Effects of the Upper Plate Velocity and the Channel Length on Oil Film Velocity

When the channel length $l = 3$ mm, based on Equation (12), the effects of the upper plate velocity on oil film velocity are analyzed, as shown in Figure 4. According to Figure 4, the oil film velocity is a parabola along the channel thickness direction. With the increase in the velocity of the upper plate, the dimensionless velocity distribution curve gradually moves downward, and the peak of the oil film dimensionless velocity gradually decreases. The reason is that the effect of the upper plate velocity on the oil film velocity is larger than that of the pressure due to the increase in the upper plate velocity, so the oil film velocity is more likely to be close to the upper plate velocity.
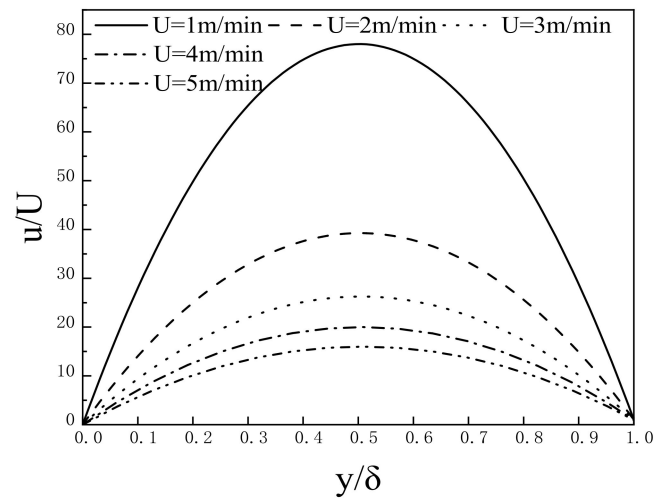
Figure 4. Effects of upper plate velocity on oil film velocity.

When the upper plate velocity $U = 1\text{m}/\text{min}$, based on Equation (12), the effects of the channel length on oil film velocity are analyzed, as shown in Figure 5. According to Figure 5, with the increase in channel length, the dimensionless velocity distribution curve gradually moves downward, and the peak of oil film dimensionless velocity gradually decreases. According to Equation (11), with the increase in the channel length, the pressure gradient gradually decreases, which leads to the effect of pressure on the oil film velocity being less than that of the upper plate velocity, so the oil film velocity is more likely to be close to the upper plate velocity. According to Figures 4 and 5, the dimensionless velocity increases at first, and then decreases with the increase in oil film thickness.
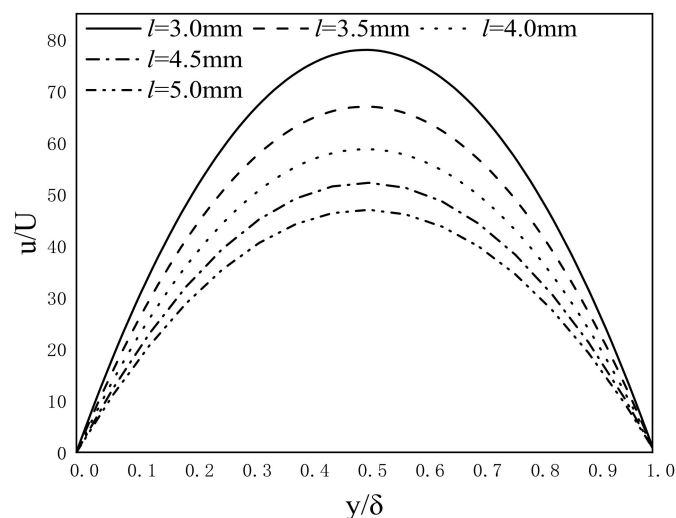

Figure 5. Effects of channel length on oil film velocity.

4.2. Effects of Inside Temperature on Oil Film Temperature

When the upper plate velocity U = 1 m/min and the inside temperature of the lower plate $T_{W1} = 20\ ^\circ\text{C}$, based on Equations (29)–(31), the effects of the channel length on oil film temperature are analyzed, as shown in Figure 6. The oil film temperature distribution can be divided into three sections: increasing zone (the temperature increases with the increase in the channel thickness y = 0–6 μm), stabilizing zone (the temperature remains unchanged with the increase in the channel thickness y = 6–14 μm), and decreasing zone (the temperature decreases with the increase in the channel thickness y = 14–20 μm). The

reasons are as follows: In the increasing zone, the temperature increases with the increase in the channel thickness due to the heat generated by friction. Then, the temperature reaches the maximum value when the channel thickness is about 6 μm and enters the stabilizing zone. The heat generated by friction increases the oil film temperature, but the inside temperature of the plate decreases the oil film temperature. The two aspects are balanced in the stabilizing zone, so the oil film temperature remains stable. In the decreasing zone, the oil film temperature decreases with the increase in the channel thickness due to the effect of the lower temperature of the upper plate. The temperature distribution curve moves downward with the increase in channel length, which means that the oil film temperature decreases. The reason is that with the increase in the channel length, the contact surface between the hydraulic oil in the channel and the inside of the plate gradually increases, leading to the oil film temperature more likely to approach the inside temperature of the plate.
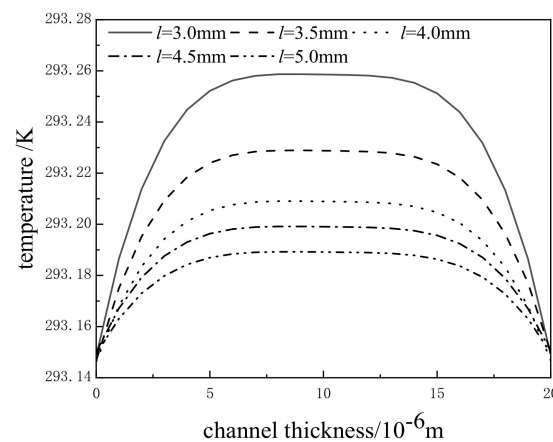

Figure 6. Effects of channel length on oil film temperature.

When the channel length l = 3 mm and the inside temperature of the lower plate T_{W1} = 20 °C, based on Equations (29)–(31), the effects of the upper plate velocity on oil film temperature are analyzed, as shown in Figure 7. When the channel thickness is less than 10 μm, the temperature distribution curve moves upward with the increase in the upper plate velocity, which means that the oil film temperature increases with it. When the channel thickness is greater than 10 μm, the temperature distribution curve moves downward with the increase in the upper plate velocity, which means that the oil film temperature decreases with it. When the channel thickness is equal to 10 μm, the oil film temperature is equal to 293.26 K. When the channel thickness is less than 10 μm, the velocity gradient increases with the increase in the upper plate velocity, so the heat generated by friction increases, then the oil film temperature is increased. When the channel thickness is greater than 10 μm, the velocity gradient is negative, so the heat generated by friction decreases with the increase in the velocity gradient, then the oil film temperature is decreased.

When the upper plate velocity U = 1 m/min and the channel length l = 3 mm, based on Equations (29)–(31), the effects of the inside temperature of the lower plate on oil film temperature are analyzed, as shown in Figure 8. According to Figure 8, with the increase in the inside temperature of the lower plate, the oil film temperature increases gradually. The reason is that the heat of the lower plate is transferred to the oil film. The higher the inside temperature of the lower plate is, the more heat is transferred to the oil film, and the oil film temperature is increased. When the inside temperature of the lower plate is constant, the oil film temperature changes little, and its fluctuation value is 0.11 K.
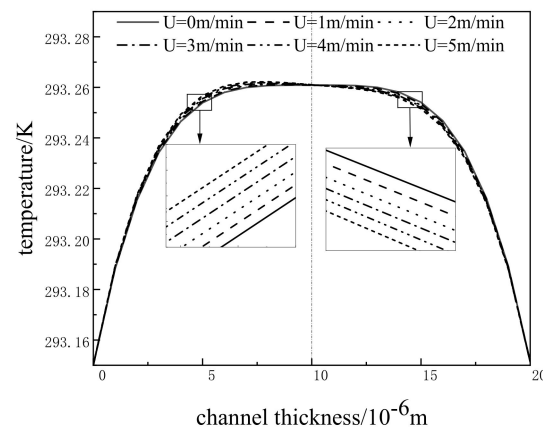
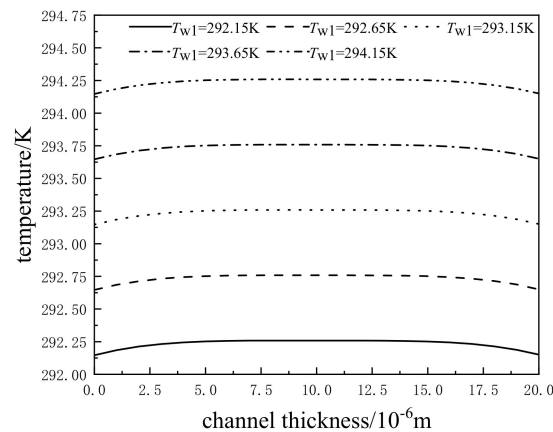**Figure 7.** Effects of upper plate velocity on oil film temperature.

Figure 8. Effects of inside temperature of lower plate on oil film temperature.

4.3. Effects of Plate Thickness and Temperature Difference on Plate Heat Flux

When the temperature difference $\Delta T = 1K$, based on Equations (33) and (34), the effects of the plate thickness (δ_1 and δ_2) on plate heat flux are analyzed, as shown in Figure 9. According to Figure 9, the heat flux decreases gradually with the increase in the plate thickness, and the relationship between the plate thickness and heat flux is linear. This phenomenon can be explained by the theory of thermal resistance. When the temperature difference is constant, the thermal resistance in the heat transfer process gradually increases with the increase in the plate thickness, so the heat flux gradually decreases. When the thickness of the upper plate increases from 0.1 m to 0.2 m, the heat flux in the upper plate decreases from 4.941 W/m to 4.884 W/m; when the thickness of the lower plate increases from 0.3 m to 0.5 m, the heat flux of the lower plate decreases from 4.828 W/m to 4.720 W/m.

When the lower plate thickness $\delta_1 = 0.3$ m and the upper plate thickness $\delta_2 = 0.1$ m, based on Equations (33) and (34), the effects of the temperature difference on plate heat flux are analyzed, as shown Figure 10. The heat flux increases linearly with the increase in the temperature difference. The plate heat flux is less than zero when the temperature difference is less than zero. When the plate thickness is constant, which means that the thermal resistance is constant, the temperature difference gradually increases, then the heat transfer force gradually increases, so the plate heat flux gradually increases. Negative temperature difference means that the air temperature is greater than the inside temperature of the lower plate, then the air heat is transferred to the plate, so the plate heat flux is less than 0. When the temperature difference increases from −1 K to 3 K, the heat flux of the

upper plate increases from −4.94 W/m to 14.82 W/m, and the heat flux of the lower plate increases from −4.83 W/m to 14.49 W/m.
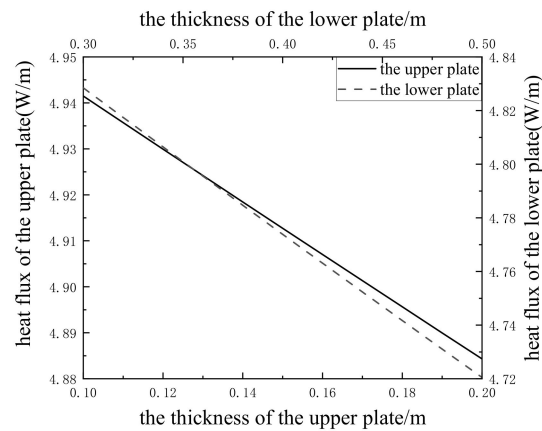

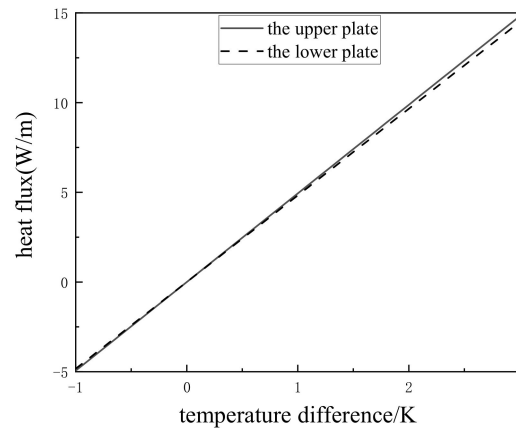**Figure 9.** Effects of plate thickness on plate heat flux.

Figure 10. Effects of temperature difference on plate heat flux.

5. Conclusions

In this article, three equations of hydrostatic oil film flowing in a flat microflow boundary layer are constructed by the theories of heat transfer and hydrodynamics, which are the velocity distribution equation, the temperature distribution equation, and the heat flux distribution equation between hydraulic oil and the surrounding air. The effects of several parameters on the velocity distribution, temperature distribution and heat flux distribution are studied, such as the upper plate velocity and the channel length. The following conclusions can be drawn:

1. The oil film velocity is a quadratic function of y and is a parabola along the channel thickness direction. The dimensionless velocity increases at first and then decreases with the increase in oil film thickness. The dimensionless velocity of the oil film decreases with the increase in the upper plate velocity and the channel length.

2. The oil film temperature is a quartic function of y. The oil film temperature distribution can be divided into three sections: the increasing zone (the channel thickness y = 0–6 μm), the stabilizing zone (y = 6–14 μm) and the decreasing zone (y = 14–20 μm). There are three influencing factors, which are the channel length, the upper plate velocity and the inside temperature of the lower plate. The oil film temperature decreases with the increase in channel length. The oil film temperature increases gradually with the increase in the inside temperature of the lower plate. When $\delta < 10$ μm, the oil film temperature increases with the increase in the upper plate velocity. When $\delta = 10$ μm,

the oil film temperature is equal to 293.26 K. When $\delta > 10$ μm, the oil film temperature decreases with the increase in the upper plate velocity.

3. The heat flux distribution is affected by the plate thickness and the temperature difference between the inside temperature of the plate and the environment temperature. The heat flux decreases linearly with the increase in the plate thickness, and increases linearly with the increase in the temperature difference. When the temperature difference increases from -1 K to 3 K, the heat flux of the upper plate increases from -4.94 W/m to 14.82 W/m, and the heat flux of the lower plate increases from -4.83 W/m to 14.49 W/m.

Author Contributions: Methodology, R.D. and T.L.; validation, L.L. (Liansheng Liu), H.Q. and T.L.; data curation, C.L., E.W. and L.L. (Lujia Liu); writing—original draft preparation, H.Q.; writing—review and editing, R.D. and T.L. All authors have read and agreed to the published version of the manuscript.

Institutional Review Board Statement: Not applicable.

Informed Consent Statement: Not applicable.

Data Availability Statement: Not applicable.

Conflicts of Interest: The authors declare no conflict of interest. The funders had no role in the design of the study; in the collection, analyses, or interpretation of data; in the writing of the manuscript, or in the decision to publish the results.

References

1. Liu, Z.F.; Zhan, C.P.; Cheng, Q.; Zhao, Y.S.; Li, X.Y.; Wang, Y.D. Thermal and tilt effects on bearing characteristics of hydrostatic oil pad in rotary table. *J. Hydrodyn.* **2016**, *28*, 585–595. [CrossRef]
2. Liu, T.; Gao, W.G.; Tian, Y.L.; Mao, K.; Pan, G.X.; Zhang, D.W. Thermal simulation modeling of a hydrostatic machine feed platform. *Int. J. Adv. Manuf. Technol.* **2015**, *79*, 1581–1595. [CrossRef]
3. Zhong, H.; Zhang, G.K. *Design Manual for Hydrostatic and Hydrodynamic-Hydrostatic Bearings*; Electronic Industry Press: Beijing, China, 2007.
4. Wang, Z.W.; Zhao, W.H.; Chen, Y.L.; Lu, B.H. Prediction of the effect of speed on motion errors in hydrostatic guideways. *Int. J. Mach. Tool. Manu.* **2013**, *64*, 78–84. [CrossRef]
5. Shao, J.P.; Dai, C.X.; Zhang, Y.Q. The effect of oil cavity depth on temperature field in heavy hydrostatic thrust bearing. *J. Hydrodyn.* **2011**, *23*, 676–680. [CrossRef]
6. Zhang, Y.Q.; Liu, G.L.; Yang, X.D.; Hu, C.Y.; Wang, H.L.; Shao, J.P. Coupled solving thermal deformation of hydrostatic bearing rotary worktable based on temperature fields of oil film. *J. Comput. Theor. Nanosci.* **2015**, *12*, 3917–3921. [CrossRef]
7. Zhang, Y.Q.; Sun, J.C.; Kong, P.R.; Kong, X.B.; Yu, X.D. The dynamic simulation and experiment of bearing capacity of multi oil cushion static bearing with double rectangular cavities. *Ind. Lubr. Tribol.* **2019**, *71*, 1072–1079. [CrossRef]
8. Zhang, Y.Q.; Yu, Z.Y.; Chen, Y.; Shao, J.P.; Yu, X.D.; Jiang, H. Simulation and experimental study of lubrication characteristics of vertical hydrostatic guide rails. *High Technol. Lett.* **2014**, *20*, 315–320.
9. Kumara, V.; Satish, C.S.; Jain, S.C. On the restrictor design parameter of hybrid journal bearing for optimum rotordynamic coefficients. *Tribol. Int.* **2006**, *39*, 356–368. [CrossRef]
10. Zamiruddin, N.E.H.; Sani, A.S.A.; Rosli, N. Oil viscosity effects on lubricant oil film behaviour under minimum quantity lubrication. *IOP Conf. Ser. Mater. Sci. Eng.* **2021**, *1092*, 012029. [CrossRef]
11. Fang, C.G.; Huo, D.H.; Huang, X.D. A comprehensive analysis of factors affecting the accuracy of the precision hydrostatic spindle with mid-thrust bearing layout. *Int. J. Adv. Manuf. Technol.* **2021**, *114*, 949–967. [CrossRef]
12. Aaron, B.C.; Noah, D.M.; Robert, E.J. Pressure measurements for translating hydrostatic thrust bearings. *Int. J. Fluid Power* **2005**, *6*, 19–24.
13. Zhu, J.; Zhang, K.; Feng, K. Experimental measurement of oil film thickness distribution in titling-pad thrust bearings by ultrasonic piezoelectric elements. *J. Vib. Eng. Technol.* **2021**, *9*, 1335–1346. [CrossRef]

14. Dou, P.; Jia, Y.P.; Wu, T.H.; Peng, Z.X.; Yu, M.; Tom, R. High-accuracy incident signal reconstruction for in-situ ultrasonic measurement of oil film thickness. *Mech. Syst. Signal. Process.* **2021**, *156*, 107669. [CrossRef]
15. Wu, C.W.; Ma, G.J. Abnormal behavior of a hydrodynamic lubrication journal bearing caused by wall slip. *Tribol. Int.* **2005**, *38*, 492–499. [CrossRef]
16. Zhang, Y.F.; Hei, D.; Liu, C.; Guo, B.J.; Lu, Y.J.; Müller, N. An approximate solution of oil film forces of turbulent finite length journal bearing. *Tribol. Int.* **2014**, *74*, 110–120. [CrossRef]
17. Deng, C.Y.; Yang, K.; Lu, S.; Chen, X.; Zhao, Y.; Ma, Y. Numerical analysis based on oil film characteristics of sliding bearing. In *Journal of Physics: Conference Series*; IOP Publishing: Orlando, FL, USA, 2021.
18. Nicodemus, E.R.; Satish, C.S. Orifice compensated multirecess hydrostatic/hybrid journal bearing system of various geometric shapes of recess operating with micropolar lubricant. *Tribol. Int.* **2011**, *44*, 284–296. [CrossRef]
19. Vijay, K.D.; Chand, S.; Pandey, K.N. Effect of different flow regime on the static and dynamic performance parameter of hydrodynamic bearing. *Procedia Eng.* **2013**, *51*, 520–528.
20. Du, Y.K.; Mao, K.M.; Zhu, Y.M.; Wang, F.Y.; Mao, X.B.; Li, B. Dynamic modeling of hydrostatic guideway considering compressibility and inertia effect. *Front. Mech. Eng.* **2015**, *10*, 78–88. [CrossRef]
21. Zhang, Y.Q.; Fan, L.G.; Li, R.; Dai, C.X.; Yu, X.D. Simulation and experimental analysis of supporting characteristics of multiple oil pad hydrostatic bearing disk. *J. Hydrodyn.* **2013**, *25*, 236–241. [CrossRef]
22. Shi, D.Y.; Shi, X.J.; Shi, X.B. Numerical computation of dynamic character coefficient of journal bearing. *Key Eng. Mat.* **2011**, *486*, 45–48. [CrossRef]
23. Zhang, Y.Q.; Li, W.W.; Fan, L.G.; Li, R.; Shao, J.P. Simulation and experimental analysis of influence of inlet flow on heavy hydrostatic bearing temperature field. *Asian J. Chem.* **2014**, *26*, 5478–5482. [CrossRef]
24. Singla, A.; Chauhan, A. Experimental evaluation of lubricating oil film pressure and temperarture of elliptical non-circular journal bearing profile. In Proceedings of the 2015 2nd International Conference on Recent Advances in Engineering & Computational Sciences (RAECS), Chandigarh, India, 21–22 December 2015.
25. Conti, R.; Frilli, A.; Galardi, E.; Meli, E.; Nocciolini, D.; Pugi, L.; Rindi, A.; Rossin, S. An efficient quasi-3D rotordynamic and fluid dynamic model of tilting pad journal bearing. *Tribol. Int.* **2016**, *103*, 449–464. [CrossRef]
26. Li, Q.; Yu, G.C.; Liu, S.L.; Zheng, S.Y. Application of computational fluid dynamics and fluid structure interaction techniques for calculating the 3D transient flow of journal bearings coupled with rotor systems. *Chin. J. Mech. Eng.* **2012**, *25*, 926–932. [CrossRef]
27. Li, M.X.; Gu, C.H.; Pan, X.H.; Zheng, S.Y.; Li, Q. A new dynamic mesh algorithm for studying the 3D transient flow field of tilting pad journal bearings. *Proc. Inst. Mech. Eng.* **2016**, *230*, 1470–1482. [CrossRef]
28. Zhang, Y.Q.; Li, W.W.; Yu, Z.Y.; Li, Q.; Shao, J.P.; Jiang, H. Flow criterion research on fluid in hydrostatic bearing from laminar to turbulent transition. *J. Inf. Technol.* **2014**, *7*, 211–216. [CrossRef]
29. Zhang, Y.Q.; Luo, Y.; Ni, S.Q.; Zhang, Z.Q. Heavy load characteristics of micro-beveled heavy-duty hydrostatic bearing lubricant oil film. *Proc. Inst. Mech. Eng.* **2021**, *235*, 738–747.